Low-temperature properties of a model glass. I. Elastic dipole model

Eric R. Grannan*
Laboratory of Atomic and Solid State Physics, Cornell University, Ithaca, New York 14853-2501

Mohit Randeria†
Department of Physics, University of Illinois at Urbana-Champaign, 1110 West Green Street, Urbana, Illinois 61801 and Materials Research Laboratory, University of Illinois at Urbana-Champaign, 104 South Goodwin Avenue, Urbana, Illinois 61801

James P. Sethna
Laboratory of Atomic and Solid State Physics, Cornell University, Ithaca, New York 14853-2501
(Received 5 May 1989; revised manuscript received 20 October 1989)

We develop a model to explain the universal low-temperature properties of glasses in the $1 < T < 10$ K temperature range. Our model consists of elastic dipole "defects" which are placed randomly in an elastic continuum. We derive a Hamiltonian for defects interacting via their long-range strain fields. We simulate a system of elastic dipoles placed on a lattice with site dilution, and find local minima of the defect Hamiltonian using Monte Carlo annealing. For a broad range of dilution, the ground states found are disordered. We study various excitations about these ground states. In this paper (I) we determine the barriers to reorientations of the dipoles, and find that these are in quantitative agreement with dielectric-loss data on the orientational glass KBr:KCN. We also compare our results with other recent theories of orientational glasses. In the following paper (II) we study harmonic excitations about the glassy ground states and the effect of these excitations on the low-temperature thermal properties; we compare our results with experimental data on KBr:KCN and vitreous silica.

I. INTRODUCTION

It has now been known for a long time[1] that amorphous materials have low-temperature properties that are markedly different from crystals, and strikingly similar to one another, independent of their structural or chemical composition. The phenomenological theory of two-level systems[2] (TLS) of Anderson, Halperin, Varma, and Phillips has been very successful in helping to understand very-low-temperature ($T < 1$ K) behavior. However, there are several questions that this theory leaves unanswered. First, there is no microscopic basis for the tunneling centers which lie at the heart of the TLS theory. Second, the TLS theory does not address the quantitative universality of certain features seen in the very-low-temperature data; these just seem to arise due to numerical "accidents" in the TLS parameters. Finally, there are universal aspects of the intermediate-temperature ($1 < T < 10$ K) data on glasses which cannot be explained even *qualitatively* within the TLS model. For example, every amorphous insulator shows a "plateau" in the thermal conductivity between 1 and 10 K, where the conductivity is essentially independent of the temperature. In addition to the plateau, the specific heat in this temperature range shows an excess over the Debye value (i.e., that obtained from the speed of sound), which is best seen as a bump in a plot of C/T^3 versus temperature. Further, all glasses show a broad (β or secondary) relaxation peak well below their freezing temperature.

In this paper (I) and its companion[3] (II) we shall focus on these intermediate-temperature universal properties of glasses. This work extends the results previously published in a short paper.[4] Our thinking has been strongly guided by one particular material, the disordered crystal $(KBr)_{1-x}(KCN)_x$, which, in its orientational glass phase, shows all of the universal low-temperature properties[5] of structural glasses. Since its microscopic structure is much better characterized than that of a "real" glass, it has the dual advantage of providing a microscopic basis for our theory and being a stringent test case for it. At a phenomenological level, we also compare our results to vitreous silica.

We summarize the results of this paper in the following.

We introduce our model in Sec. II. We begin with an elastic continuum containing randomly placed defects. The simplest characterization of a defect which couples to a strain field is an elastic dipole, and we have taken this as the basis of the model. Specializing to a traceless uniaxial dipole, and neglecting local fields, leaves only one parameter to characterize a single defect For KBr:KCN these assumptions can be justified on microscopic grounds. For a more general glass, our model must be considered phenomenological. In the rest of this paper and its companion we will analyze this model and show that it is rich enough to give rise to the universal intermediate-temperature properties of glasses.

In Sec. III we develop the elasticity theory for dipole

defects coupled to the phonon modes of the medium and use it to derive a Hamiltonian for defects interacting via their strain fields. We make a major simplifying approximation by taking the phonons to be fast on the time scale of the defect excitations. The validity of this approximation is assessed in II, where we study the harmonic defect modes. While much of what we say in Sec. III is available in the literature, we are careful in treating the $\mathbf{k}=0$ strain mode and in our treatment of periodic boundary conditions.

We next describe in Sec. IV our numerical simulation of the defect Hamiltonian. We use a Monte Carlo heat-bath method followed by a zero-temperature quench to find local energy minima, or ground states, of a system of dipoles placed on a lattice with site occupation probabilities x of 0.25, 0.5, and 0.7.

We discuss the nature of the ground states obtained in the various simulations in Sec. V, and find that, for a range of defect densities, these are glasslike. For $x=0.25$ and 0.5, the ground states seem not to exhibit long-range order. The dipoles point in random directions (with some short-range order in a $\langle 111 \rangle$ direction) determined by the local strain field. At concentration $x=0.7$, the system *does* have long-range order, in the $Pa3$ structure, but many of its properties still look glassy.

We study in Sec. VI a particular excitation about the glassy ground state: a 180° flip of a single dipole, which is a local excitation connecting two degenerate ground states. We compare the barrier heights for these reorientations with two recent models for orientational glasses. The distribution of barriers is reasonably approximated by a Gaussian, except for the low-barrier tail, which shows a hole presumably due to level repulsion. In Sec. VII we study the same reorientations, allowing the neighboring dipoles to relax. We compare the barrier heights thus obtained with dielectric-loss data in KBr:KCN. We obtain quite good agreement at all concentrations, with the barrier-height distribution determined from the dielectric loss.

Finally, in Sec. VIII we discuss the relation of our work to previous theoretical work. The discussion of theories of the low-temperature properties of glasses is left to II; here we discuss our model in the context of other microscopic models of alkali halide alkali cyanides.

In II, we study harmonic excitations about the glassy ground states of the defect Hamiltonian. We treat the coupling of long-wavelength phonons to these defect modes within perturbation theory. We calculate the specific heat and thermal conductivity of our disordered system and find characteristic glassy behavior in the intermediate temperature regime. We compare our results with experiments on KBr:KCN and vitreous silica. For the latter case, the parameters are fixed by matching the defect density of states to recent neutron-scattering experiments by Buchenau *et al.*[6]

Readers primarily interested in the low-temperature *thermal* properties of glasses may wish to turn to II after reading Sec. II of the present paper.

II. MODEL

At long wavelengths a glass has well-defined elastic constants. In addition, there is clear experimental evidence for the presence of nonphonon degrees of freedom. In specific-heat measurements one sees an additional source of entropy; in thermal transport, which is experimentally known to be phonon dominated,[7] one sees evidence for strong phonon scattering, especially in the 10^{12}-Hz frequency region.

On rather general grounds, one way in which glasses differ from crystalline materials is that they have a distribution of internal stresses due to the disorder inherent in their structure. These internal stresses give rise to internal motions which are clearly different from the phonons.

We model these internal stresses in terms of "defects" in an elastic continuum. It should be stressed that the notion of isolating these "defects" at the microscopic level in a real glass is, in general, not well defined; what is the defect and what is the medium? Thus, this type of model can only be used for structural glasses in a phenomenological way. However, as we shall show below, for a system such as KBr:KCN we can provide a detailed microscopic justification for our model.

A single defect in an elastic medium is characterized by an elastic multipole expansion[8] in much the same way as in, say, electrostatics. The source for displacements in an elastic medium is a point force. Symmetry does not allow for an elastic monopole since this would be a unbalanced force, so, in general, the strain field that dies away most slowly with distance ($1/r^3$) is that due to the elastic dipole moment. In analogy with an electric dipole, an elastic dipole is given by two opposing forces whose strength goes to infinity as their separation goes to zero. An elastic dipole[8,9] is characterized by a symmetric second-rank tensor; the antisymmetric part represents an unbalanced torque.

We make three simplifying assumptions about the dipole defects. First, we will consider traceless defects, which means that there is no volume change due to the dipole. The trace of an elastic dipole couples only to longitudinal phonons, whereas, experimentally, transverse phonons are equally strong scattered, and even for longitudinal phonons the relative volume change that would be required to account for the measured phonon-defect coupling is unphysically large. Second, we restrict ourselves to the case where two of the axes are equal, i.e., the dipole is cylindrically symmetric. Third, since we would like to have a model with the minimum number of free parameters, we take all the defects to be identical, rather than having a distribution of dipole moments.

Given these assumptions, only one number, Q_0, the elastic dipole moment, is needed to characterize the energies of the defect.[10] Each elastic dipole is then given by $Q_{ij}=Q_0(\hat{n}_i\hat{n}_j-\frac{1}{3}\delta_{ij})$, where $\hat{\mathbf{n}}$ is a unit vector. (The terminology in the field is rather confusing and, by analogy with electrostatics, Q_{ij} is sometimes called a "quadrupole"; we will always call it an elastic dipole.) This dipole can be pictured as looking like an ellipsoid placed in a spherical hole in a block of rubber. It pushes out in one direction, and pulls in in the other two directions. As we define it, the elastic dipole has units of energy and couples to the strain field in the host medium.

We must now address the issue of what determines the dynamics of these defects. We will assume that the only

important interaction is the strain-mediated coupling between the elastic dipoles, which is described in Sec. III. We use linear-elasticity theory to calculate this interaction. At short distances, comparable to a lattice spacing, the use of linear elasticity is in itself an approximation, which we nevertheless make on grounds of simplicity. In general, an isolated defect will have preferred orientations due to the local environment. We neglect all such effects, so that an isolated dipole in our model behaves like a free symmetric rotor. For KBr:KCN, as we will discuss below, this assumption appears to be well justified, insofar as the intermediate-temperature properties are concerned. For the more general case, even the separation of the interaction into "exchange" (defect-defect) and "local-field" (defect-local cage) pieces is not well defined.

We will discuss in more detail in II the extent to which the neglect of local-field effects is justified. It is probably worthwhile to ask what would happen if we took the completely opposite point of view from the one taken in this paper, ignoring all interactions between defects and assuming that the dynamics is determined only by local-field effects. In that case, an analysis identical to the one given in Ref. 11 shows that if the local-field distribution (which is not known in general glasses) is treated as adjustable, one can obtain the usual intermediate-temperature properties of glasses. Of course, in reality it would be impossible to turn off the phonon-mediated interaction between defects, while keeping a finite defect-phonon coupling as required by the thermal conductivity. Local-field effects, however, *are* indeed negligible in some glassy systems, like, e.g., KBr:KCN. Thus, at the very least, our model raises a nontrivial question: Is it possible to get the universal intermediate-temperature properties of glasses from the simplest model, which only has the phonon-defect interaction?

A. KBr:KCN

We now turn to a brief discussion of the disordered crystal KBr:KCN which, after all, was the inspiration for the model, and is a material for which we can make fairly direct comparisons between our results and experiment. In particular, we will point out the microscopic basis for some of the simplifying assumptions made above.

$(KBr)_{1-x}(KCN)_x$ can be made with any concentration x of CN^-'s, spanning the range between pure KBr and pure KCN. For x between about 0.1 and 0.6, the CN^-'s freeze into random orientations (as has been shown by neutron scattering[12]) which do not have long-range orientational order. Over this range of composition the material exhibits all the usual low-temperature glassy properties:[5] linear specific heat and T^2 thermal conductivity below 1 K, a thermal-conductivity plateau, a broad dielectric-loss peak,[13] etc.

We make the obvious association between the cyanide ions which randomly replace the bromines on the anion sublattice and the elastic dipoles of our model. For simplicity, we ignore all higher-order elastic multipoles. The approximation of neglecting the volume shift due to the cyanides (i.e., ignoring the trace of the dipole tensor) is a very good one since the lattice constant of $(KBr)_{1-x}(KCN)_x$ is essentially constant as x is varied, for $x \lesssim 0.6$ (above this concentration, the material has a ferroelastic phase transition at low temperatures).

There are (at least) three energy scales relevant to the cyanides. These are due to the *elastic* interaction between the cyanides, the *electric* interaction between the cyanides, and the interaction between the cyanide and the crystal field of the host lattice. The crystal-field-energy scale can be estimated from experiments on very dilute (a few ppm) cyanide concentrations in a KBr host lattice. In this case the CN^-'s point in the eight $\langle 111 \rangle$ directions and have barriers of 5 K between different orientations.[14] The other two energy scales can be estimated from KCN, where at zero temperature the barrier to 180° reorientations[14] is 1855 K and the asymmetry energy[15] is 340 K. From this, we see that for moderate to high cyanide concentration the elastic interactions between cyanides are dominant. Thus it is reasonable from a microscopic standpoint to treat KBr:KCN as a system of interacting elastic dipoles.

We should also mention that there are some differences between our model and the real material KBr:KCN. The ground state at high concentration ($x \sim 1$) is different: $(KBr)_{1-x}(KCN)_x$ at this concentration is in a ferroelastic phase at low temperatures, and in our simulation we find a $Pa3$ structure (see Sec. V). This difference may be due to the neglect of higher-order elastic multipoles, or of local-field effects. Of course, our main interest is in the lower-concentration glassy phase. In the glassy phase, KBr:KCN has cubic elastic constants, but in our model we have taken the elastic constants to be isotropic. Simplifying the detailed interaction in this way has conceptual as well as computational advantages. Since the properties we are trying to understand occur in all glasses as well as KBr:KCN, one hopes that the details of the interaction do not play a major role.

For KBr:KCN we can get all the microscopic parameters of our model from experiment. In addition to the elastic constants, these are the elastic dipole moment, the moment of inertia of a cyanide ion, and the density of defects.

III. DEFECT HAMILTONIAN

Our aim is to simulate a disordered system of elastic dipoles interacting via their strain fields. In general, second-rank tensors will interact through a Hamiltonian of the form

$$H = -\frac{1}{2} \sum_{\substack{\mathbf{x},\mathbf{x}' \\ (\mathbf{x} \neq \mathbf{x}')}} J_{ijkl}(\mathbf{x},\mathbf{x}') Q_{ij}(\mathbf{x}) Q_{kl}(\mathbf{x}') , \tag{1}$$

and specifically, for elastic dipoles, J will be the strain field at $\mathbf{x}$ caused by a dipole at $\mathbf{x}'$. The main thrust in this section is the determination of J_{ijkl}.

We will use periodic boundary conditions in our simulation. To consider the effects of such a periodic system in a systematic way, we will reformulate the problem below and write a "full Hamiltonian" which explicitly includes the phonon modes of the elastic medium in addition to the defects. We will eventually want to include

phonons in our model to study the thermal and transport properties, and it will be useful to have a Hamiltonian which includes them explicitly. This is different from the standard method of elasticity, in which the phonons are always considered to be fully relaxed. We will rederive in this way the Fourier-space equations for the strain field of a dipole.

The phonons mediate an effective interaction between dipoles. We will see that besides the $1/r^3$ strain field around each dipole, minimizing the energy in the $\mathbf{k}=\mathbf{0}$ mode leads to a uniform strain field. This strain field vanishes for a single dipole in an infinite medium, but in a system with a finite density of dipoles it only costs a finite amount of energy per dipole. The uniform strain field is important since it can cause a ferroelastic transition to a state where there is a long-wavelength deformation, and the dipoles all line up. It also must be treated correctly, even in the absence of a long-wavelength deformation, in order to study the response of the system to externally applied stresses.

We should point out that the Hamiltonian studied in this paper incorporates two aspects of the strain-mediated interaction between dipoles that were neglected in our earlier work.[4] First, we did not include the $\mathbf{k}=\mathbf{0}$ uniform strain mode in Ref. 4. This makes no difference in the interaction energy of two *isolated* elastic dipoles, because it costs an infinite amount of energy to have a uniform strain field in an infinite medium. However, for a *finite concentration* of defects the energy cost per defect of such a strain field is finite. Thus it is necessary to include its contribution to $J_{ijkl}(\mathbf{x})$. Second, we had previously used periodic boundary conditions with a sharp cutoff on the interaction at the size of the box. In this paper we impose true periodic boundary conditions, so that a given elastic dipole interacts with *all* the periodic images of the other dipoles. We will show that these changes do not qualitatively modify the results of Ref. 4.

A. Phonon-defect Hamiltonian

We want to obtain the Hamiltonian for a system of elastic dipole defects interacting with the strain field in a finite elastic medium with periodic boundary conditions.

We begin by writing the most general strain field, which is periodic in a cube of side L:

$$\varepsilon_{ij}(\mathbf{r})=\frac{1}{2}\left[\frac{dP_i}{dx_j}+\frac{dP_j}{dx_i}\right]+e_{ij} , \tag{2}$$

where the $P_i(\mathbf{r})$ are periodic, and the e_{ij} are arbitrary symmetrized constants. This is just the strain field obtained from a displacement field $u_i(\mathbf{r})$ which has a periodic part $P_i(\mathbf{r})$ and a linear part of the form $e_{ij}r_j$.

Expanding the P_i in a Fourier series,

$$P_i(\mathbf{r})=\sum_{\mathbf{k}}\tilde{u}_i(\mathbf{k})e^{i\mathbf{k}\cdot\mathbf{r}}, \quad \mathbf{k}=\frac{2\pi}{L}(n_1,n_2,n_3) \tag{3}$$

with n_i integers, we obtain the strain field,

$$\varepsilon_{ij}(\mathbf{r})=\sum_{\mathbf{k}}\tilde{\varepsilon}_{ij}(\mathbf{k})e^{i\mathbf{k}\cdot\mathbf{r}} , \tag{4}$$

where

$$\tilde{\varepsilon}_{ij}\equiv\begin{cases}e_{ij}, & \mathbf{k}=\mathbf{0}\\ (i/2)(k_i\tilde{u}_j+k_j\tilde{u}_i), & \mathbf{k}\neq\mathbf{0} .\end{cases} \tag{5}$$

Note that the $\mathbf{k}=\mathbf{0}$ mode has to be treated separately, and cannot be obtained from the $\mathbf{k}\to\mathbf{0}$ limit of the finite-$\mathbf{k}$ part. While the six $\mathbf{k}=\mathbf{0}$ components e_{ij} can be chosen independently, for $\mathbf{k}\neq\mathbf{0}$, $\tilde{\varepsilon}_{ij}(\mathbf{k})$ are *not* six arbitrary continuous functions since they must be derived from a physical (i.e., continuous, single-valued) displacement field.

The elastic energy stored in these strain fields is

$$E_{\rm el}=\int\tfrac{1}{2}c_{ijkl}\varepsilon_{ij}(\mathbf{r})\varepsilon_{kl}(\mathbf{r})dV , \tag{6}$$

where c_{ijkl} is the elastic-constant tensor. (For a review of elasticity theory, see, e.g., Refs. 16 and 17.) Converting this to a sum over the Fourier modes gives

$$E_{\rm el}=\frac{V}{2}\sum_{\mathbf{k}}c_{ijkl}\tilde{\varepsilon}_{ij}(\mathbf{k})\tilde{\varepsilon}^{*}_{kl}(\mathbf{k}) . \tag{7}$$

If we apply a force to a point in an elastic continuum, the continuum will respond so as to minimize the total energy. For a given displacement, we gain an energy equal to $-\mathbf{F}\cdot\mathbf{u}$. An elastic dipole, being a pair of opposed forces, will couple to the derivative of the displacement, that is, to the strain field. So, considering a pair of forces whose separation goes to zero, keeping the product of force times separation constant, we get that the interaction energy between a dipole and a strain field is given by

$$E_{\rm int}=-Q_{ij}\varepsilon_{ij} . \tag{8}$$

We can now write the "full" Hamiltonian for an elastic medium including the interaction with embedded dipoles located at sites $\mathbf{x}$. The (potential-energy part of the) Hamiltonian is then

$$H_{\rm full}=\sum_{\mathbf{k}\,(\neq 0)}\left[\frac{V}{8}c_{ijkl}(k_i\tilde{u}_j+k_j\tilde{u}_i)(k_k\tilde{u}^{*}_l+k_l\tilde{u}^{*}_k)-\sum_{\mathbf{x}}\frac{i}{2}(k_i\tilde{u}_j+k_j\tilde{u}_i)Q_{ij}(\mathbf{x})e^{i\mathbf{k}\cdot\mathbf{x}}\right]+\frac{V}{2}c_{ijkl}e_{ij}e_{kl}-\sum_{\mathbf{x}}e_{ij}Q_{ij}(\mathbf{x}) . \tag{9}$$

The first and third terms represent the elastic energy of the medium in the finite-$\mathbf{k}$ modes and in the uniform modes, respectively. The second and fourth terms represent the energy of interaction between the elastic dipole defects located at $\mathbf{x}$ and the strain fields.

B. Elastic Green functions

Before finding the interaction energy between two elastic dipoles, it is convenient to begin by computing the Green function for the strain field due to a dipole source.

We will assume that the phonon-mediated interaction between dipoles can be taken as instantaneous. For this approximation to be valid, it is necessary that motions of the defects be slow on the time scale characteristic of the phonons ($1/\tau_{\text{defect}} \ll \omega_{\text{Debye}}$). This approximation is checked in II, where we study the defect modes. Since τ_{defect} depends on the parameters of the model, so does the validity of this approximation. We will find that for the parameters relevant to KBr:KCN, neglecting retardation effects is only marginally justified, whereas for silica there is a clear separation of time scales. More generally, we believe that it is reasonable, as a first approximation, to neglect retardation effects in the study of this model.

We now specialize to an isotropic medium, with Lamé coefficients λ and μ. In this case

$$c_{ijkl}^{\text{iso}} = \lambda\delta_{ij}\delta_{kl} + \mu(\delta_{ik}\delta_{jl} + \delta_{il}\delta_{jk}) \ . \tag{10}$$

We can then obtain[18] the Green function for the strain field of a dipole by minimizing the total energy (9) with respect to the phonon coordinates,

$$\tilde{\varepsilon}_{ijkl}(\mathbf{k}) = \frac{1}{V\mu}\left[\tfrac{1}{4}(\delta_{ij}\hat{k}_k\hat{k}_l + \delta_{ik}\hat{k}_j\hat{k}_l + \delta_{lj}\hat{k}_k\hat{k}_i + \delta_{lk}\hat{k}_j\hat{k}_i) - \left[\frac{\lambda+\mu}{\lambda+2\mu}\right]\hat{k}_i\hat{k}_j\hat{k}_k\hat{k}_l\right] \tag{11}$$

(where $\hat{\mathbf{k}}$ is a unit vector) for $\mathbf{k}\neq\mathbf{0}$. The $\mathbf{k}=\mathbf{0}$ strain field is given by

$$\tilde{\varepsilon}_{ijkl}(\mathbf{k}=\mathbf{0}) = \frac{1}{V}\frac{1}{2\mu}\left[\tfrac{1}{2}(\delta_{ik}\delta_{jl} + \delta_{il}\delta_{jk}) - \left[\frac{\lambda}{3\lambda+2\mu}\right]\delta_{ij}\delta_{kl}\right] = \frac{1}{V}s_{ijkl} \ , \tag{12}$$

where the compliance tensor $s_{ijkl} = c_{ijkl}^{-1}$ is the inverse of the elastic modulus tensor. $\tilde{\varepsilon}_{ijkl}$ has been made manifestly symmetric under interchange of $i\leftrightarrow j$, $k\leftrightarrow l$, and $ij\leftrightarrow kl$. In fact, these symmetries are true in general, not just for an isotropic material. [Formulas analogous to (11) and (12) can also be obtained for a cubic material; see Ref. 18.]

For an isolated dipole in an infinite medium only the $\mathbf{k}\neq\mathbf{0}$ modes contribute to the strain field, as argued earlier. In this case (11) can be Fourier-transformed to real space to obtain

$$\varepsilon_{ijkl}(\mathbf{r}) = \frac{1}{8\pi\mu}\left[-\tfrac{1}{2}(\delta_{ik}\partial_{jl} + \delta_{il}\partial_{jk} + \delta_{jk}\partial_{il} + \delta_{jl}\partial_{ik})\left[\frac{1}{r}\right] + \left[\frac{\lambda+\mu}{\lambda+2\mu}\right]\partial_{ijkl}(r)\right] \ , \tag{13}$$

where we use ∂_{ij} for $\partial^2/\partial x_i \partial x_j$. From this it is apparent that the strain field of a dipole dies off like $1/r^3$.

More generally, when we have a finite density of defects, we must include the $\mathbf{k}=\mathbf{0}$ mode as well. We then obtain the real-space Green function J_{ijkl} for the strain of a dipole,

$$J_{ijkl}(\mathbf{x}) \equiv \sum_{\mathbf{k}} \tilde{\varepsilon}_{ijkl}(\mathbf{k}) e^{i\mathbf{k}\cdot\mathbf{x}} \ , \tag{14}$$

where $\tilde{\varepsilon}_{ijkl}(\mathbf{k})$ are given by (11) and (12). The resulting strain field at $\mathbf{r}$ due to an elastic dipole at the origin is then given by

$$\varepsilon_{kl}(\mathbf{r}) = J_{ijkl}(\mathbf{r}) Q_{ij}(\mathbf{0}) \ . \tag{15}$$

C. Interaction between defects

The interaction energy between two elastic defects in a medium is defined[19] to be the energy of the two sources minus the contribution each defect would have made in the absence of the other. This energy can be calculated by minimizing the energy in the phonon modes.[18] Here we give a simple argument which gives the same result.

To determine the interaction energy between two forces, consider a material with a body force embedded in it, and then turn on a second-body force. The interaction energy is given by the difference between the work we do with the second force present, and the work that we would do if it were absent. As we turn on the second force, by linearity the displacement in the medium will simply add to the displacement already present. So the only difference in the work done with a force present is due to that part of the work done as in moving the first force. The interaction energy is then $-\mathbf{F}(1)\cdot\mathbf{u}(2)$.

The interaction energy between two dipoles is obtained in a similar way, by turning on an elastic dipole in the presence of the strain field due to another dipole. This gives $E_{\text{int}} = -Q_{ij}(1)\varepsilon_{ij}(2)$.

We get the following effective Hamiltonian for a system of elastic dipoles,

$$H_{\text{eff}} = -\tfrac{1}{2}\sum_{\substack{\mathbf{x},\mathbf{x}' \\ (\mathbf{x}\neq\mathbf{x}')}} Q_{ij}(\mathbf{x}') J_{ijkl}(\mathbf{x}-\mathbf{x}') Q_{kl}(\mathbf{x}') \ , \tag{16}$$

where the real-space Green function J_{ijkl} for the strain of a dipole is given by (14). Note that since J_{ijkl} is symmetric between exchange of ij and kl, $Q_{ij}(1)\varepsilon_{ij}(2) = Q_{ij}(2)\varepsilon_{ij}(1)$. The interaction energy of a system of dipoles is thus given by a sum of pair interactions. Equation (16) is the main result of this section; this is the equation that all of our simulations will involve. Since J_{ijkl} has been calculated by summing the appropriate Fourier modes, this Hamiltonian implicitly imposes periodic boundary conditions.

Let us conclude with some comments on the interaction between two elastic dipoles. The $\mathbf{k}\neq\mathbf{0}$ part leads to an anisotropic $1/r^3$ interaction, as seen in (13). It can be shown[18] analytically that for two isolated dipoles a "tee"

configuration is a local minimum of this interaction. In this configuration one dipole is pointing in the direction of the vector separating the two and the other is perpendicular to it. Numerically we find that the "tee" appears to be the global minimum. The uniform $\mathbf{k}=\mathbf{0}$ part of the interaction has the rather different effect of making two dipoles align parallel to each other. The combined effect of these interactions on the ground states of a system of interacting dipoles will be discussed later.

IV. SIMULATION

One possible approach to study this system would be through a mean-field theory. As is known from the study of Ising spin glasses, as well as work on quadrupolar glasses,[20] a rigorous mean-field theory for systems with quenched disorder is quite difficult, and we have chosen instead to perform a numerical simulation.

The basic purpose of the simulation is to find "ground states" of the interaction Hamiltonian (16). By a ground state, we mean a low-energy local minimum of the Hamiltonian, not necessarily a global minimum. Since we are dealing with a disordered system and are trying to model a glass, we do not expect that there should be one particular ground state that is much lower in energy than any other local minimum. We have also investigated the ground-state structure of a small system in some detail and find that there are, in fact, many competing local minima of similar energy. (This, together with a study of the zero-temperature entropy of the system, will be discussed in a separate publication.[21])

We have chosen to run a Monte Carlo simulation to find ground states. Alternatively, we could have just performed a minimization of the energy, using a steepest-descent algorithm. An advantage of using a Monte Carlo simulation is that we expect to find better ground states than by merely going straight downhill, as one is less likely to get trapped in a high-energy metastable configuration.

In the simulation we cycle through the dipoles repeatedly, in a random order each time. The strain field at each dipole is calculated. We then pick an orientation $\hat{\mathbf{n}}$ for that dipole from a Boltzmann distribution (the heat-bath method). The temperature is slowly lowered to zero until the system converges into a local minimum of the energy.

At zero temperature we want to go to the minimum of whatever energy valley we happen to be in. To do this, we go through the dipoles one at a time,[22] and align them with the local strain field until the system converges. We consider the system to have converged if the fractional change in energy is less than some small value, typically 10^{-12}.

The quenched randomness in our Hamiltonian (16) is in the random location of the dipoles. To obtain a random configuration, we take each site in a finite fcc lattice, and place a dipole with probability x at that site (that is, we have site dilution). We have typically used $5\times5\times5$ conventional fcc unit cells, which gives 500 total sites. We have performed simulations with $x=0.25$, 0.5, and 0.7. We average over typically 10–20 different random configurations to determine properties for a given concentration. The simulation was performed on the IBM 3090 computer at the Cornell National Supercomputer Facility, and we used about an hour of central-processing-unit (CPU) time for each run, including the Monte Carlo annealing, calculation of relaxed barrier heights (Sec. VII), and diagonalization of the dynamical matrix (see II).

Before we run the simulation, we calculate the $J_{ijkl}(\mathbf{x})$ tensor for each possible displacement vector $\mathbf{x}$ between lattice sites. Note that for a given set of elastic constants and a given lattice size, we only have to calculate $J_{ijkl}(\mathbf{x})$ once, and we can then use the same values of J_{ijkl} in other runs of the simulation regardless of the positions of the dipoles or of the concentration. When running the simulation, we then use the $J_{ijkl}(\mathbf{x})$ previously calculated. The J_{ijkl}'s are obtained by Eq. (14), summing[23] over the $\mathbf{k}$ values dictated by the periodic boundary conditions. This has the effect of including the interaction of a given dipole with *all* the periodic images of other dipoles.

We do *not* include the interaction of a dipole with its own images. Including this would make the Monte Carlo simulation more difficult, since the energy would no longer be of the form $-\varepsilon_{ij}(\mathbf{x})(\hat{n}_i\hat{n}_j-\frac{1}{3}\delta_{ij})$, with $\varepsilon_{ij}(\mathbf{x})$ independent of $\hat{\mathbf{n}}$. The effect of interacting with your own images (in a cubic array) can be shown to be equivalent to adding a crystal field of the form

$$A(x^4+y^4+z^4)\,, \tag{17}$$

where A can be either positive or negative, depending on the elastic constants. We have chosen to neglect this interaction for two reasons. First, the effect of interacting with one's own images is clearly unphysical and disappears in the limit of an infinite system. Second, since we have already decided to neglect local-field interactions, it seems defensible to throw this one away as well.

Finally, a word on the units used in our simulations. On the computer, we consider the fcc conventional unit cells to be one unit on a side, and the elastic dipole moment of the dipoles to be 1. The elastic constants are given to the computer, and we will see that only the ratio of the elastic constants matters to the results. The *magnitudes* of the elastic constants are chosen after the simulation to match to experiment. Unless otherwise mentioned, the results we will discuss in this section were obtained on a $5\times5\times5$ lattice with $\lambda=\mu=1.0$. These numbers have been chosen because their ratio, 1.0, is the ratio of λ and μ given by the Voigt spherical average[17] of the elastic constants (i.e., isotropically averaging the elastic modulus tensor, rather than the compliance tensor) for KBr. We will give energies mainly in "computer units" in this section. As a scale to the energy, in the ground state of the system with dipoles on all the sites of a fcc lattice, and with these elastic constants, the energy per dipole is equal to -0.557, and the barrier to the reorientation of a dipole is 1.67. The procedure by which we go from the computer units to physical units requires the use of formalism developed in II, and is thus described there.

V. GROUND-STATE STRUCTURE

As discussed earlier (at the end of Sec. III), the preferred orientation for two dipoles in an isotropic medium

is a "tee," i.e., one dipole is parallel, and the other is perpendicular to the vector connecting them. This "tee" configuration is frustrated on a fcc lattice; even if we were to approximate the interaction by limiting it to near neighbors, the dipoles could not satisfy all their bonds simultaneously. The "tee" configuration is actually frustrated on any three-dimensional Bravais lattice. This can be seen by considering two neighbors in the, say, $\hat{\mathbf{x}}$ direction from each other (see Fig. 1). One (dipole 1) must be pointing in the $\hat{\mathbf{x}}$ direction, and the other (dipole 2) in a perpendicular direction, say the $\hat{\mathbf{y}}$ direction. Then dipole 2 must have a neighbor in the $\hat{\mathbf{y}}$ direction (dipole 3) which must be pointing in the x-z plane. Since dipole 2 has a neighbor in the $\hat{\mathbf{y}}$ direction, dipole 1 must also have a neighbor (dipole 4) in that direction, which must point in the $\hat{\mathbf{y}}$ direction. Then dipoles 3 and 4 must be neighbors, so dipole 3 must actually point in the $\hat{\mathbf{x}}$ direction. This pattern can be repeated in two dimensions to form a two-dimensional rectangular lattice on which all bonds are satisfied. Now, all the neighbors in the $\hat{\mathbf{z}}$ direction must be pointing in the $\hat{\mathbf{z}}$ direction in order to satisfy the bonds with neighbors in the original plane. But in doing so, they do not satisfy the interactions within the second plane. This shows that the "tee" interaction cannot be satisfied on a three-dimensional Bravais lattice. Since the real interaction is long ranged, the question of when the (approximate) near-neighbor interaction is frustrated is of only marginal interest, and we will not pursue it further.

A. Nondiluted systems

Considering the long-range interaction again, we now discuss the structure of the ground state for a system in which dipoles are placed on *all* of the fcc lattices sites, i.e., the site occupation probability $x=1$. For an isotropic elastic medium, there are two possible structures depending on the ratio of the elastic constants λ and μ.[24] If λ/μ is greater than about -0.385, the lowest-energy configuration is the $Pa3$ structure, which is well known[25] from solid ortho-hydrogen. In this structure the dipoles of each of the four simple-cubic sublattices pick a different $\langle 111 \rangle$ (body diagonal) direction in which to point, with the condition that near-neighbor dipoles do not lie in the same plane. There are eight degenerate $Pa3$ structures. We have conducted most of our simulations with isotropic elastic constants with $\lambda=\mu=1.0$. This structure differs from KCN at low temperatures, which has an orthorhombic structure, with the long axes of the cyanides pointing in a direction corresponding to a $\langle 110 \rangle$ direction in a cubic lattice.

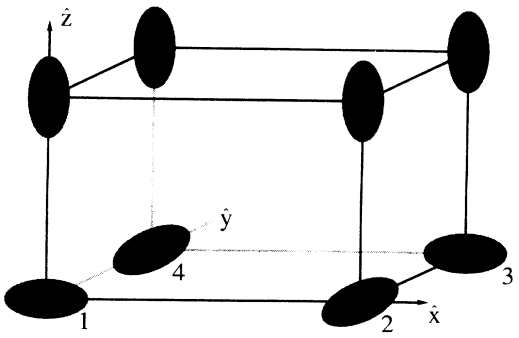

FIG. 1. Elastic dipoles are frustrated in a three-dimensional Bravais lattice.

For λ/μ less than -0.385, the dipoles line up in one of the $\langle 100 \rangle$ directions. By lining up in the same direction, the dipoles can take advantage of a large uniform strain field, although the rest of the interaction energy is positive.

We have checked that anisotropic elastic constants are not sufficient to reproduce the correct ground-state structure for KCN, by running the simulation using cubic elastic constants.[18] Using the elastic constants for KBr as our bare elastic constants, however, it turns out that the $x=1$ system prefers the same state as the isotropic case, that is, the $Pa3$ state. Among the ferroelastic states—that is, states with the dipoles all pointing in the same direction—the best one is not even the $\langle 110 \rangle$ state, but the $\langle 111 \rangle$ state. Perhaps ignoring the higher multipoles may be responsible for our model having the "wrong" ground state in the ordered limit $x=1$.

B. Dilute systems

We find that the properties of the ground states do not depend on the rate of cooling over the range of rates that we can practically achieve. We also find that if we cool the same system many times we find different ground states. In fact, unless the system is very small (on the order of 20 dipoles), we never get the same ground state twice.

At the lowest two concentrations, the states we end up with look glassy, with only short-range correlations in the orientations of the dipoles. For $x=0.7$, the systems have strong correlations throughout the lattice, showing definite tendencies of the $Pa3$ structure. In Fig. 2 we

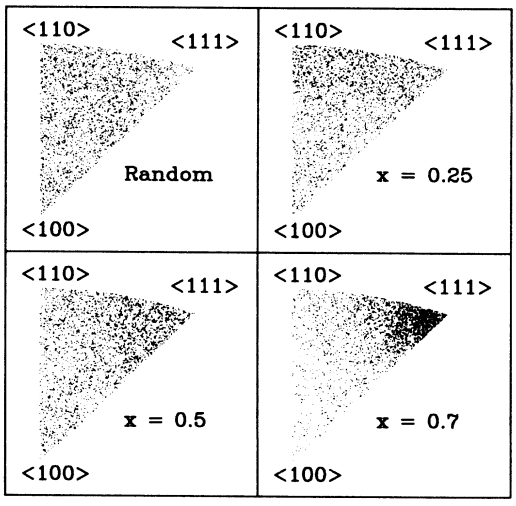

FIG. 2. Orientations of the dipoles in the ground states for three concentrations—0.25, 0.5, and 0.7. Also shown for comparison is a random distribution of the same number of points. The points have been folded onto a wedge of the sphere using the operations of the cubic symmetry group, and then projected in an area-preserving manner onto a plane.

show a scatter plot of the orientations of the dipoles. We create this by first folding the orientations of the dipoles, using the cubic group operations, onto a wedge containing $\frac{1}{48}$ of the sphere. We have then projected the wedge from three-dimensional space onto a plane, in a manner so that area is preserved. We see that for concentrations 0.25 and 0.5, the distribution of orientations is fairly uniform over the wedge, with some tendency to point in the $\langle 110 \rangle$ and $\langle 111 \rangle$ directions. For concentration 0.7, there is a quite strong tendency to point in a $\langle 111 \rangle$ direction.

Another simple way to look at the structure of the system is to consider the correlations between the orientations of the dipoles. In Figs. 3–5 we show the distribution of relative orientations of dipoles at various distances from each other. If the orientations were uncorrelated, the distributions would all be flat. For the *Pa*3 structure, the distribution would be δ functions at $\frac{1}{3}$ for the distances whose square is a half-integer, and δ functions at 1 for distances whose square is an integer. We see that for the lower two concentrations there are fairly weak correlations between the orientations of the dipoles.

For $x=0.7$ the systems have strong correlations throughout the lattice. The structure is quite reminiscent of the *Pa*3 structure, with signs of the peak at $\frac{1}{3}$ and a very strong peak at $\cos\theta=1$ for the distances whose square is an integer. At this concentration in $(KBr)_{1-x}(KCN)_x$, the cyanides have undergone a ferroelastic transition, so (as in our simulation) their orientation is no longer random, but the ground state is different from the one that we get.

Despite the long-range order, the $x=0.7$ results do show some features which are glassy. The normal modes of the dipoles at this concentration (discussed in II) do not look extended, at least at the high- and low-frequency tails, unlike the $x=1$ case. The distribution of barrier heights (discussed in the next section) is broad, with a

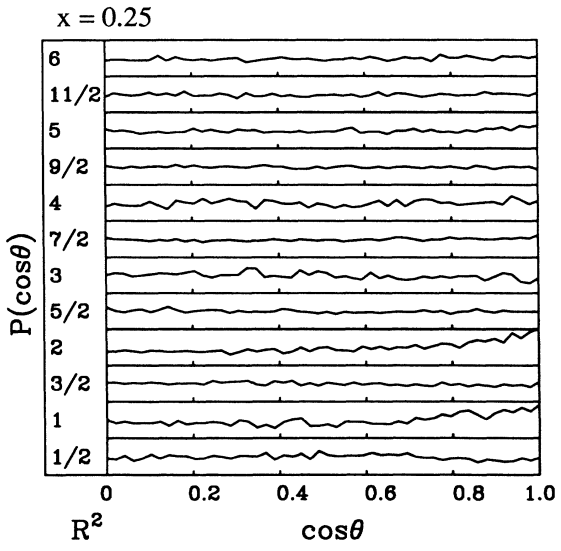

FIG. 3. Probability distributions for the relative angles θ between dipoles plotted as a function of $\cos\theta$. The concentration is $x=0.25$. Each of the 12 plots is for a different separation R between the dipoles, measured in units of a fcc unit cell whose side length is 1. Dipoles whose squared displacement is an integer are on the same simple-cubic sublattice; otherwise they are on different sublattices. At concentration 0.25 the correlations are rather weak, although there is some tendency for dipoles on the same sublattice to line up.

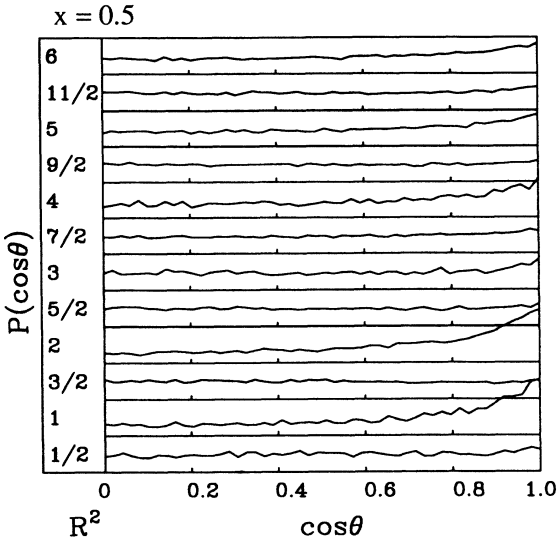

FIG. 4. Same as Fig. 3, at concentration $x=0.5$. Here there is a tendency for dipoles on the same sublattice to line up at short distances, which appears to be dying away for dipoles separated by the largest distance.

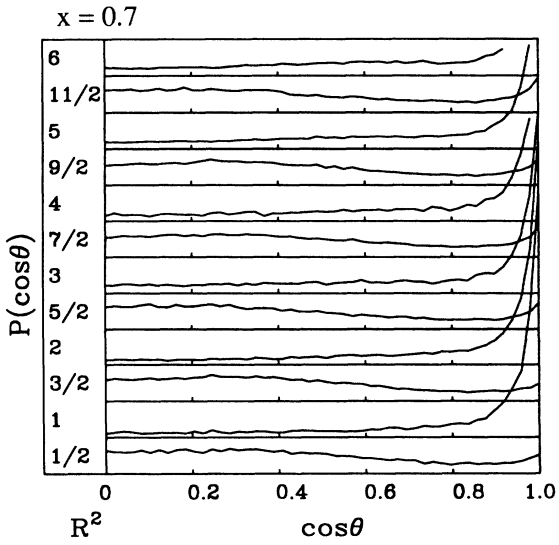

FIG. 5. Same as Fig. 3, at concentration $x=0.7$. At this concentration the system exhibits long-range orientational order in the *Pa*3 structure, signaled by peaks in $P(\cos\theta)$ at $\cos\theta=1$. Dipoles on the same lattice have a strong tendency to line up, and dipoles on separate lattices tend to be arranged with $\cos\theta=\frac{1}{3}$. Despite the orientational order, we will see that this system has some properties which look glassy.

similar width as at $x=0.5$. Furthermore, even though the dipiles tend to point in $\langle 111 \rangle$ directions, as is shown in Fig. 2, there is a large amount of disorder in the direction in which they choose to point.

VI. BARRIER HEIGHTS

We now study the distribution of barrier heights to 180° reorientations of the dipoles. There are several reasons why these barriers are of interest. First, in our model, the configuration when a dipole has flipped by 180° is degenerate with the unflipped configuration. Thus a 180° reorientation of a single dipole is a natural local excitation. A broad distribution of barrier heights is characteristic of a glassy system; for a concentration $x=1$, the distribution of barriers is given by a δ function, as all the dipoles have the same environment. Second, dielectric-loss experiments[13] in $(KBr)_{1-x}(KCN)_x$ have been interpreted in terms of distributions of barrier heights, and we will be able to compare the distributions that we obtain with the experimental distributions.

In KBr:KCN the two-level systems have been considered[26] to be those cyanides (about one in 10^5) which happen to have a very low barrier to reorientation, so that they can quantum-mechanically tunnel on experimental time scales. In principle, it should be possible to look for these two-level systems in our simulation, but, practically, the true TLS would be so rare that they would not be seen in a simulation of achievable size. Consequently, we cannot say anything in detail about TLS.

Another reason that barrier heights are of interest is that there have been two recent theoretical calculations of distributions of barrier heights in "quadrupolar" glasses. The two groups analyzed somewhat different models, both of which simplify the actual elastic dipole interaction, and which embody different aspects of the physics present in real materials. Sethna and Chow[27] (SC) have calculated a mean-field theory for a model which ignored the frustration of the elastic dipole interaction, but included the effect of dilution, the fact that different dipoles have different numbers of near neighbors.

Kanter and Sompolinsky[20] (KS) have performed a replica mean-field theory of a model which is frustrated, but in which all the dipoles are equivalent, and each dipole interacts with all the other dipoles.

There are two barriers which we will calculate. In this section we discuss the "bare" barrier; that is, the barrier to the reorientation of a particular dipole when all the other dipoles are fixed. This is given by Q_0 times the difference between the largest two eigenvalues of the strain tensor evaluated at the dipole. This is the barrier height discussed in the theoretical calculations. In the following section we will discuss the distribution of barrier heights when other dipoles are allowed to relax.

The model Hamiltonian studied by Kanter and Sompolinsky was

$$H_{\mathrm{KS}} = -\sum_{\mathbf{x},\mathbf{x}'} K_{klmn}(\mathbf{x},\mathbf{x}')Q_{kl}(\mathbf{x})Q_{mn}(\mathbf{x}') , \tag{18}$$

where the components of $K_{klmn}(\mathbf{x},\mathbf{x}')$ are independent random variables aside from the usual symmetries; that is, $K_{klmn}=K_{lkmn}=K_{mnkl}$. The sum is over all pairs of dipoles, so each dipole interacts with all the other dipoles with a coupling drawn from the same distribution. They obtained a *replica-symmetric* solution, valid above the temperature where the dipoles tend to freeze into a general orientation, and a solution with *replica-symmetry breaking*, valid below the freezing temperature and down to zero temperature. A distinctive feature of both of these solutions is that the distribution $P(V)$ goes to zero linearly as $V\rightarrow 0$.

Our model differs from this model in several ways. In the first place, our J_{ijkl} tensors are not random. The randomness in our model is due to the random location (dilution) of the dipoles, not from any randomness inherent in the interaction. Furthermore, the interaction tensor for a pair of dipoles in our model is a function of the difference in position of the dipoles, and since we place the dipoles on a lattice, many pairs of dipoles will be separated by the same displacement vector and therefore have the same J_{ijkl}. Similarly, the J_{ijkl} values even for different displacement vectors will not be uncorrelated. Since the J_{ijkl} tensors are correlated with each other, if the orientations of the dipoles are also correlated, which certainly happens at high concentrations, the relevance of the KS model may be questionable. On the other hand, if the interaction is long ranged, one might imagine that the effects of dilution and random interactions would be the same.

The Hamiltonian of the model studied by Sethna and Chow[27] was

$$H_{\mathrm{SC}} = -\tfrac{1}{2}J \sum_{\langle ij \rangle} Q_{kl}(i)Q_{kl}(j)\chi_i\chi_j , \tag{19}$$

where the sum is over near neighbors, and $\chi_i=1$ if a site is occupied, and zero otherwise. This model ignores frustration and its ground state is highly ordered, since the energy is minimized when all the dipoles are aligned. The model does include the fact that different dipoles are in different environments, one may have many near neighbors, and another will have few neighbors. Presumably this will have a substantial effect on the barrier height seen by these two dipoles. In the mean-field-theory solution to this model the distribution of barrier heights is very nearly a Gaussian (actually a binomial distribution).

We first compare the barrier heights to the high-temperature replica-symmetric solution. In Fig. 6 we show the bare-barrier-height distribution for a system of dipoles in which the orientation of each dipole is simply chosen randomly. This corresponds to the instantaneous barrier distribution at very high temperature, where the dipoles are practically freely rotating. The high-temperature behavior of our model agrees very well with the KS replica-symmetric solution. This solution has one parameter, which sets both the width and the peak of the distribution, and which we have fitted to the distribution from the simulation.

At low temperatures our simulation converges into a local minimum of the energy. Figures 7–10 show the distribution of bare barrier heights in the ground states for

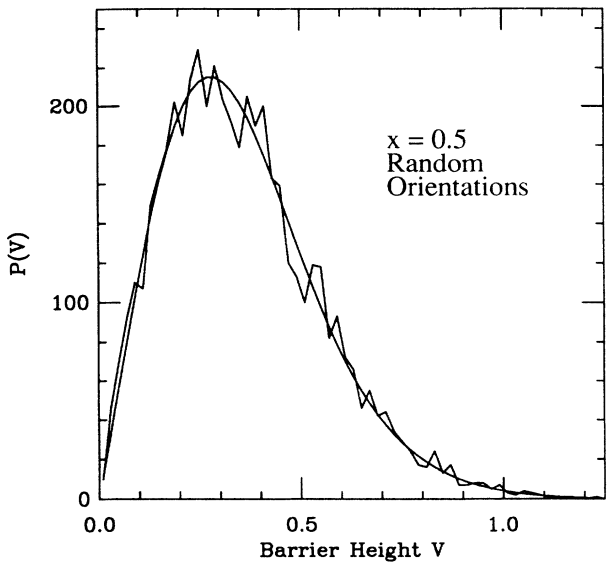

FIG. 6. Distribution of barrier heights at concentration $x=0.5$ for dipoles pointing in random uncorrelated directions. This is therefore the instantaneous barrier-height distribution at a very high temperature, where the barrier is defined as the difference between the largest two eigenvalues of the local strain-field tensor. The smooth curve is the Kanter-Sompolinsky replica-symmetric solution.

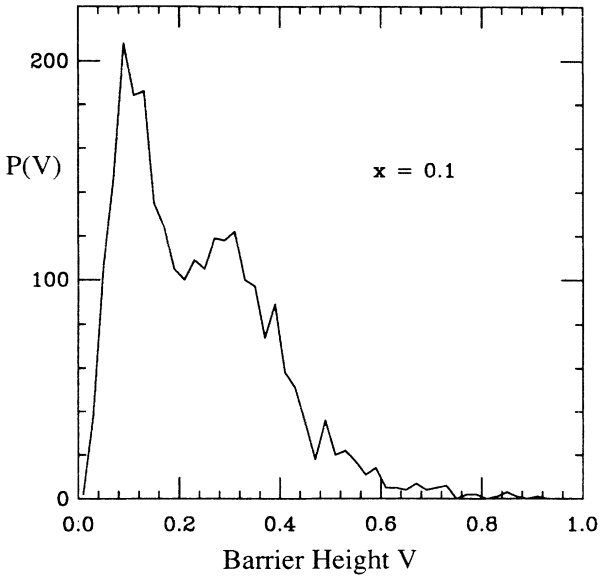

FIG. 7. Distribution of barrier heights for ground states at concentration $x=0.1$. This was done on a $6\times6\times6$ conventional unit-cell lattice. The discreteness of the lattice is becoming apparent at this low concentration. An isolated near-neighbor pair of dipoles would have barriers of 0 and 0.225.

concentrations 0.1, 0.25, 0.5, and 0.7. The distributions of the higher three concentrations are compared to both the KS replica-symmetry-breaking solution and to a Gaussian distribution. Note that the Gaussian distribution has one more parameter than the KS solution, since for the Gaussian distributions we are independently choosing both a width and mean.

At a concentration of 0.25 the KS solution gives rather good agreement with the barriers from the simulation. The quality of the fit is about the same as that of the Gaussian, even though the KS solution has one less parameter.

At both higher and lower concentrations, however, the KS solution does not do as well. We know, in fact, that at a concentration of 1.0 the distribution of barriers is a δ function, since all the dipoles will have the same environment. The question is whether, as x becomes lower, the distribution goes to the KS solution. At both of our higher concentrations, $x=0.5$ and 0.7, the KS solution is much wider than the numerical barrier distribution. This is probably due to correlations in the orientations at these concentrations. At a very low concentration of $x=0.1$ (which was done on a slightly larger $6\times6\times6$ lattice) the distribution of barrier heights is no longer given by a smooth featureless curve, and we have not attempted to fit it to either the KS solution or a Gaussian. There are two noticeable peaks at about 0.1 and 0.3, which occur since the discreteness of the lattice makes certain arrangements of dipoles likely. For example, if two dipoles are near neighbors on this lattice, and do not interact with anything else, they have barrier heights of 0.0 and 0.225. The difference between these two values agrees well with the observed difference between the two peaks of the distribution.

We find from our simulation that the barrier distribution $P(V)\rightarrow0$ as $V\rightarrow0$. Since the bare barrier height is defined by a difference in eigenvalues of a random matrix, this is just the phenomenon of level repulsion, as em-

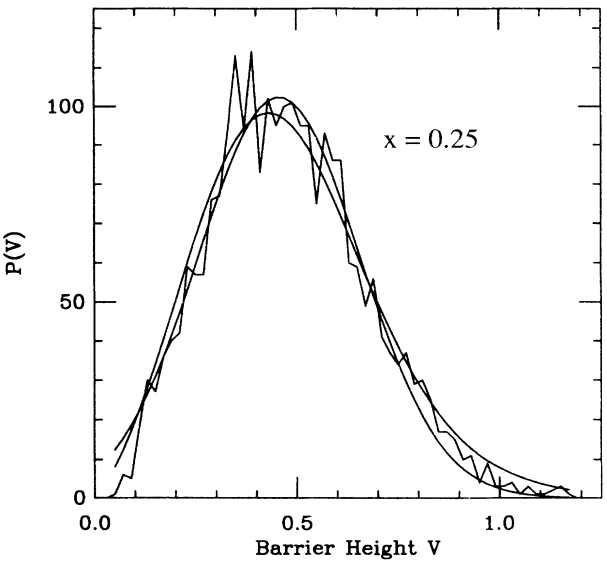

FIG. 8. Distribution of barrier heights for ground states at concentration $x=0.25$. The smooth curves are the broken-replica-symmetry solution of Kanter and Sompolinsky (which goes to zero at $V=0$) and a Gaussian (which is nonzero at $V=0$). Both curves fit the numerical barrier distribution fairly well, but the KS solution has only one free parameter, whereas the Gaussian has two.

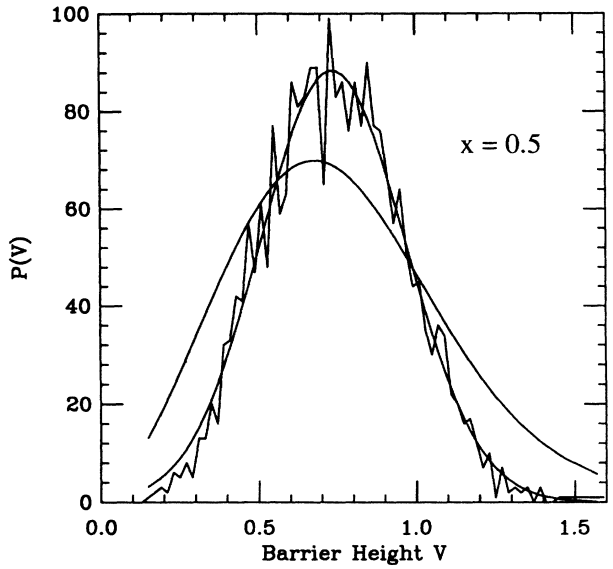

FIG. 9. Distribution of barrier heights for ground states at concentration $x=0.5$. The broad curve is the replica-symmetry-breaking solution of Kanter and Sompolinsky, and the narrow curve is a Gaussian.

phasized by KS in the present context. However, the KS solution further predicts that $P(V)$ should go to zero linearly as $V\rightarrow 0$. From the distribution of barrier heights from the simulation, we cannot, of course, rule out the possibility that the extremely low barrier tail goes to zero linearly, but if it does it must happen at such low barriers and for so few dipoles that, at least for those properties which involve a significant number of the dipoles, it would not have a noticeable effect. Furthermore, at the very low barrier tail (in the real world), local crystal-field contributions to the barrier (which both theories that we have discussed, as well as our simulation, have neglected) will become important. It also should be noted that we clearly contradict the SC solution in which the barrier distribution went to a constant as $V\rightarrow 0$.

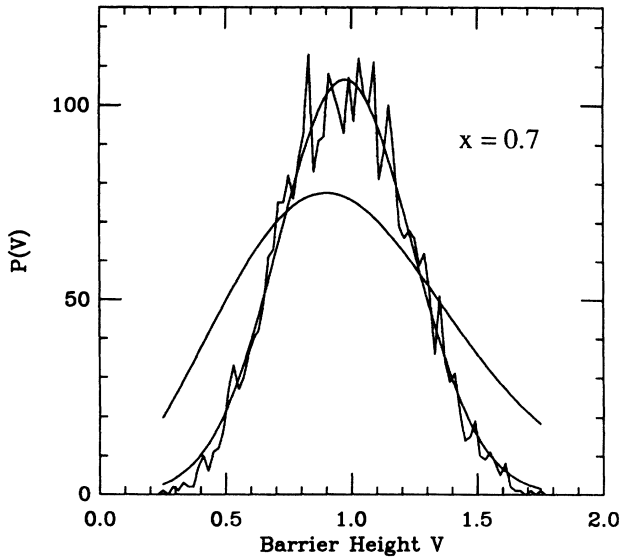

FIG. 10. Distribution of barrier heights for ground states at concentration $x=0.7$. The broad curve is the replica-symmetry-breaking solution of Kanter and Sompolinsky, and the narrow curve is a Gaussian.

TABLE I. Ratio of the width σ to the peak position μ of the barrier-height distribution. The ratios are the experimental distribution in KBr:KCN, determined from dielectric loss, the ratio for the binomial with 12 near neighbors, and the relaxed and unrelaxed barriers from the simulation.

	Ratio σ/μ			
x	Expt.	Binomial	Relaxed	Unrelaxed
0.25	0.40	0.50	0.43	0.43
0.50	0.32	0.29	0.38	0.31
0.70	0.28	0.19	0.36	0.28

If we assume that the Gaussian comes from a binomial distribution from a random number of near neighbors, as in the mean-field theory of SC, the ratio of the width to the peak position as a function of x is given by a binomial distribution. The ratios of σ/μ from the dielectric-loss experiments of Birge *et al.*, from the simulation, and from a binomial distribution are given in Table I. The ratios of the binomial distribution are qualitatively correct, but they predict somewhat too steep a change in the ratio as the concentration is changed. This is presumably due

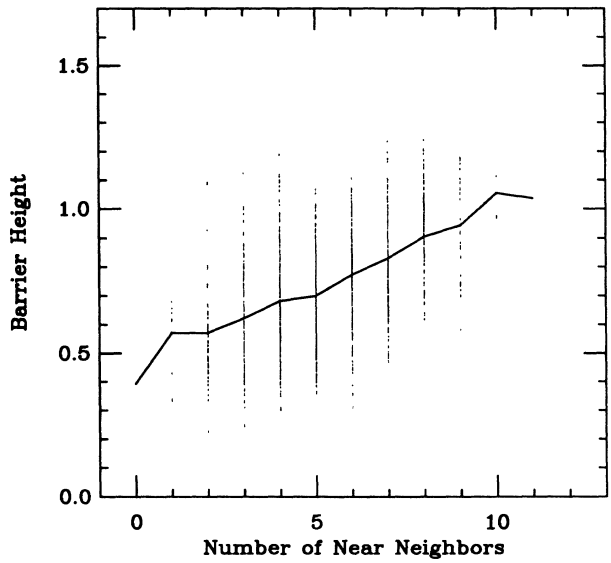

FIG. 11. Scatter plot of the barrier height as a function of the number of near neighbors for $x=0.5$. The mean of the distribution has a linear dependence on the number of near neighbors, but the width is extremely large, and there is a large intercept on the y axis. The graphs for $x=0.25$ and 0.7 (not shown) look qualitatively similar. In the Sethna-Chow theory a plot of barrier height vs number of near neighbors is a straight line through the origin.

TABLE II. Coefficients of linear fit to the bare barrier height as a function of the number of first, second, and third neighbors; that is, $V(n_1,n_2,n_3)=a_0+a_1n_1+a_2n_2+a_3n_3$. The distribution itself is actually very broad, and does not resemble a line.

x	a_0	a_1	a_2	a_3
0.25	0.271	0.089	0.007	−0.009
0.5	0.516	0.064	0.012	−0.015
0.7	0.613	0.075	0.027	−0.023

to the effects of more distant dipoles.

A way of estimating the effect of various numbers of neighbors is to consider the barrier height as a function of the number of neighbors; see Fig. 11. We have performed a least-squares fit of the barrier height as a function of the number of near, next-near, and third neighbors to the form

$$V(n_1,n_2,n_3)=a_0+a_1n_1+a_2n_2+a_3n_3 \ . \tag{20}$$

This gives the coefficients shown in Table II. As can be seen, the effect of the number of near neighbors has a large, but not overpowering, influence. The importance of the number of near neighbors is most important for the low-concentration, $x=0.25$, run (Fig. 12). The coefficient of the third-neighbor term is negative. The presence of third neighbors frustrates the closer neighbors and tends to give a lower barrier height.

VII. "RELAXED" BARRIER HEIGHTS AND DIELECTRIC LOSS

A characteristic feature in glasses is a broad distribution of relaxation times at low temperatures (i.e., well below the glass transition), known as the β relaxation. This relaxation typically spans many decades in frequency. In KBr:KCN this β relaxation has been seen through dielectric-loss measurements by Birge, Nagel, Wu, and collaborators.[13] In these experiments the coupling of the small *electric* dipole moment of the CN^- to an external time-varying electric field is used to probe the interactions between cyanides which are dominated by *elastic* forces. The dielectric-loss peak is very broad, spanning around 10 decades of frequency. The data can be fitted very well by assuming that it is due to independent degrees of freedom thermally activated over a Gaussian distribution of barrier heights.

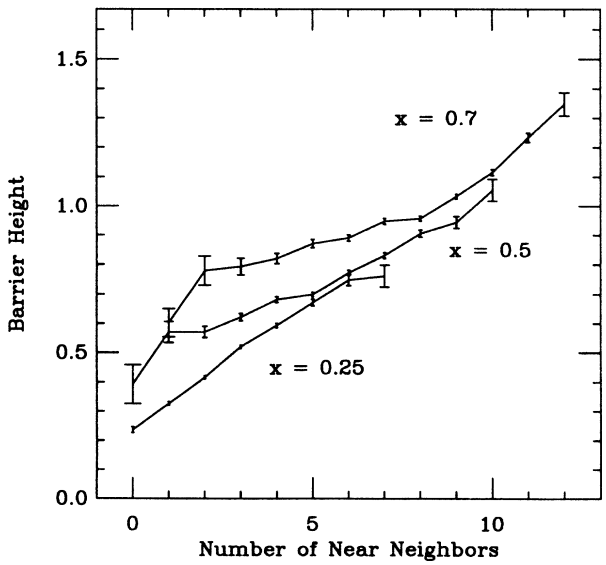

FIG. 12. The mean and error of the mean for the bare barrier height as a function of near neighbors for $x=0.25$, 0.5, and 0.7. The top line of the graph, 1.67, is the barrier height in the crystalline state at $x=1.0$.

By assuming that the excitations over these barriers are 180° reorientations of the elastic dipoles, we are able to compare the barrier distribution from the simulation with the experimental distribution. One indication that the dielectric loss in the disordered material is due to 180° reorientations is that this loss peak evolves continuously as x is reduced from the dielectric-loss peak in KCN associated with 180° reorientations.[28]

The bare barrier calculated above is actually an upper limit to the measured barrier height, since presumably the other dipoles will relax as one dipole flips over. If the process is thermally activated, as the distribution measured experimentally in KBr:KCN is, the barrier important for the reorientation rate of a dipole will be given by the lowest-energy saddle that the system has to go through as one dipole reorients itself. We therefore also calculate a "relaxed" barrier height, where we allow the other dipoles to adjust as a given dipole flips over. The effect of relaxation is not small; there is generally a large difference, of about a factor of 2, between the bare and relaxed barriers.

The idea of a relaxed barrier is somewhat ill defined. There is clearly a question of time scales involved in determining what exactly should be relaxed; relaxing an arbitrarily large number of neighbors corresponds to waiting a very long time. Furthermore, since we are dealing with a glassy system, there are lots of local minima that the system can fall into. If we try to do a very good job of finding the minimum energy barrier needed to be crossed in reorienting one dipole, we will likely find some convoluted path that goes through other local minima. This transition then cannot be considered as involving a simple reorientation of one dipole. Therefore, in searching for a relaxed barrier, there will have to be some compromise between relaxing everything and between restricting the ways in which we relax the system. It is certainly true that more complicated rearrangements of dipoles may be important experimentally; presumably single-dipole reorientations are just a particularly simple example of more general rearrangements of the system. In particular, in the $CO/N_2/Ar$ system it has been shown[29] that reorientations are not important in determining the specific heat. In this paper, however, we will only consider barriers to 180° reorientations.

We calculate the relaxed barrier heights as follows. We first constrain the dipole of interest to point in a plane perpendicular to its ground-state orientation. Although there is no guarantee that the maximum energy

should occur at $\pi/2$, all of the barriers we found using other methods[18] had their maximum barrier at $\pi/2$, so this does not seem to be a bad assumption. We then relax *some* of the other dipoles as well as the dipole whose barrier we are calculating, still requiring, of course, that it be perpendicular to its ground-state orientation. Once the system converges, we check that the whole system relaxes back into the original ground-state orientation. We have tried various groups of "other dipoles" to relax, ranging from just the near neighbors to all of the dipoles in the simulation. The problem with relaxing all the dipoles, besides being quite time consuming, is that the system not infrequently (one time in 10 or so, and more at low concentrations) ends up in a configuration which does not relax back into the original ground state. This means that we have really produced some point on a path between a more complicated rearrangement of the dipoles, not just a reorientation of a single dipole.

As a compromise, we have chosen to minimize the dipoles out to third neighbor. This distance includes 42 lattice sites. We chose relaxing out to third neighbor because the barrier that this method gives is essentially the same as the barrier height that we get when relaxing all the dipoles for those barriers that relax back into the same state. Benefits of relaxing dipoles out to third neighbor are that this method is more likely to relax back into the original state, and that it is much faster than relaxing dipoles on all 500 of the lattice sites.

A. Comparison with experiments

In order to compare the "relaxed" barrier heights with those obtained from the dielectric-loss experiments, we have to convert our results from "computer units" to physical units. While a discussion of this conversion will be taken up in II, we consider it worthwhile to present the final results here. The energy scale of the simulation is set by one number, Q_0^2/Ca^3, where C is an elastic constant and a is a typical distance between dipoles. We have used the value of 1.3 eV for the elastic dipole moment Q_0, which is consistent[30] with experiments on isolated cyanides in a KBr host. In addition, we also need to match[31] the elastic constants of the simulation to the experimentally measured value for KBr:KCN.

We plot the relaxed barrier heights from the simulation and the barrier heights deduced from the dielectric-loss experiments in Fig. 13. All the distributions agree reasonably well. It is rather surprising that the barrier heights for $x=0.7$ agree moderately well, since (as we discussed in Sec. V) the structure of the two systems is different at this concentration. It should be noted that if we are allowed to adjust the energy scale (by a factor of about 2), the unrelaxed barrier heights also fit the dielectric loss quite well; the effect of relaxation is basically just to lower the energy scale. The parameters of the various barrier-height distributions (unrelaxed, relaxed, etc.) are compared with the experiment in Table I.

In summary, a model involving 180° flips of the defect dipoles convincingly explains the dielectric-loss data. While there is clearly a correlation of the barrier heights with the number of nearest neighbors, as in the Sethna-

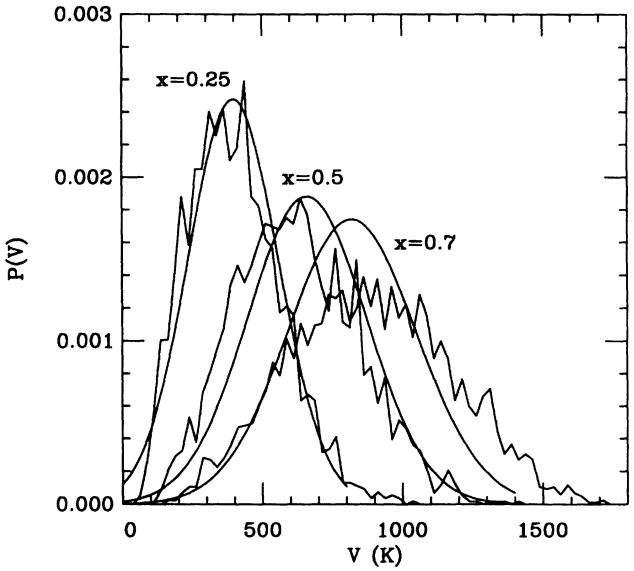

FIG. 13. Barrier heights from dielectric-loss experiments (Ref. 13) and from the simulation.

Chow analysis,[27] the effects of frustration and of more distant neighbors are also important.

VIII. RELATION TO OTHER MODELS

Our main aim in this paper and its companion (II) is to study the universal low-temperature properties of glasses. Thus far, we have discussed only certain thermally activated reorientation processes here, and have compared our results with predictions from other theories of "quadrupolar" glasses in Sec. VI. We will discuss the thermal properties of our model in II. Thus we will postpone discussion of other theories of the universal low-temperature properties to that paper.

Since our most direct comparisons with experiment are made with the glassy crystal KBr:KCN, it is appropriate here to discuss previous theoretical studies of the mixed alkali halide cyanides. Most of this work has been done from a perspective quite different than ours. These studies take a more microscopic point of view and have been concerned with the details of the crystal structure, treating all the alkali ions, halogens, and the cyanides explicitly. Michel and Rowe[32] have used interatomic potentials to derive a Hamiltonian which includes couplings between cyanides and phonons (the translational-rotational coupling), as well as single cyanide orientation potential. Their Hamiltonian includes the phonon-mediated interaction between dipoles that we have used, as well as other interactions which we have neglected. They have then studied many of the high-temperature properties, e.g., the phase transition into a disordered state, and neutron-scattering line shapes. In a similar spirit, Sahu and Mahanti have investigated phonon softening in the high-temperature phase.[33] Michel[34] has pointed out the importance of random-field effects due to the size of the halogen atoms in understanding details of the phase dia-

gram of mixed crystals. Molecular-dynamics simulations, which have been used to investigate the structural properties of alkali cyanides, have been performed by Lewis and Klein.[35] Using interatomic potentials, they are able to achieve quite good agreement with the phase diagram, as well as give insight into the structure of the disordered state.

Our interest is in the low-temperature properties, and in the excitations about the disordered ground states. Since we study properties which are universal to all glasses, we hope that these properties will be substantially independent of the details of the Hamiltonian. We have thus chosen to work with a simple model, which views the cyanide as a "defect" in a continuum, and neglects its microscopic environment. We have already shown above the the barrier heights obtained from our model are in excellent agreement with the data obtained from the dielectric-loss β-relaxation peak in KBr:KCN. To what extent this model explains the universal low-temperature properties will be discussed in the next paper.

ACKNOWLEDGMENTS

We would like to thank Paul Goldbart, Chris Henley, Tony Leggett, Sid Nagel, Bobby Pohl, Nandini Trivedi, and Clare Yu for helpful conversations. We gratefully acknowledge support by U.S. National Science Foundation (NSF) Grant No. DMR-82-17227-A01 through the Materials Science Center at Cornell University, and by NSF Grant No. DMR-86-12860 at the University of Illinois. One of us (E.R.G.) was partially supported by the NSF. The numerical simulations were done using the Cornell National Supercomputer Facility, a resource of the Center for Theory and Simulation in Science and Engineering at Cornell University, which is funded in part by the NSF, the State of New York, and the IBM Corporation.

---

*Present address: AT&T Bell Laboratories, 600 Mountain Avenue, Murray Hill, NJ 07974-2070.

†Permanent address: Department of Physics, State University of New York at Stony Brook, Stony Brook, NY 11794-3800.

[1]R. C. Zeller and R. O. Pohl, Phys. Rev. B **4**, 2029 (1971).

[2]*Amorphous Solids, Low Temperature Properties,* edited by W. A. Phillips (Springer-Verlag, Berlin, 1981).

[3]E. R. Grannan, M. Randeria, and J. P. Sethna, this issue, the following paper, Phys. Rev. B **41**, 7793 (1990).

[4]E. R. Grannan, M. Randeria, and J. P. Sethna, Phys. Rev. Lett. **60**, 1402 (1988).

[5]J. J. De Yoreo, W. Knaak, M. Meissner, and R. O. Pohl, Phys. Rev. B **34**, 8828 (1986), and references therein.

[6]U. Buchenau, H. M. Zhou, N. Nucker, K. S. Gilroy, and W. A. Phillips, Phys. Rev. Lett. **60**, 1318 (1988); U. Buchenau, M. Prager, N. Nucker, A. J. Dianoux, N. Ahmad, and W. A. Phillips, Phys. Rev. B **34**, 5665 (1986).

[7]M. P. Zaitlin and A. C. Anderson, Phys. Rev. B **12**, 4475 (1975).

[8]C. Teodosiu, *Elastic Models of Crystal Defects* (Springer-Verlag, Berlin, 1982).

[9]A. S. Nowick and W. R. Heller, Adv. Phys. **12**, 251 (1963).

[10]In II (Ref. 3), where we consider the dynamics of the defects, we also need the moment of inertia I of a defect. We will see that for the thermal properties the parameters Q_0 and I always occur together in the form $\Upsilon \equiv Q_0^2/I$, so that a defect can still be characterized by just one parameter, Υ.

[11]M. Randeria and J. P. Sethna, Phys. Rev. B **38**, 12 607 (1988); M. Randeria, Ph.D. thesis, Cornell University, Ithaca, NY, 1987.

[12]J. M. Rowe, J. J. Rush, D. J. Hinks, and S. Susman, Phys. Rev. Lett. **43**, 1158 (1979).

[13]N. O. Birge, Y. H. Jeong, S. R. Nagel, S. Bhattacharya, and S. Susman, Phys. Rev. B **30**, 2306 (1984); L. Wu, R. M. Ernst, Y. H. Jeong, S. R. Nagel, and S. Susman, *ibid.* **37**, 10 444 (1988).

[14]F. Lüty, in *Defects in Insulating Crystals,* edited by V. M. Turkevich and K. K. Swartz (Springer-Verlag, Berin, 1982), p. 69.

[15]S. Nagel (private communication), quoted in M. Meissner *et al.*, Phys. Rev. B **32**, 6091 (1985).

[16]L. D. Landau and E. M. Lifshitz, *Theory of Elasticity* (Pergamon, New York, 1959).

[17]J. P. Hirth and J. Lothe, *Theory of Dislocations* (Wiley, New York, 1982).

[18]E. R. Grannan, Ph.D. thesis, Cornell University, Ithaca, NY, 1989.

[19]J. D. Eshelby, in *Solid State Physics,* edited by H. Ehrenreich, F. Seitz, and D. Turnbull (Academic, New York, 1956), Vol. 3, p. 79.

[20]I. Kanter and H. Sompolinsky, Phys. Rev. B **33**, 2073 (1986).

[21]S. A. Langer, J. P. Sethna, and E. R. Grannan, Phys. Rev. B **41**, 2261 (1990).

[22]In general, minimizing a function by minimizing one degree of freedom at a time, cycling through the coordinates repeatedly, is not very efficient. In our case, however, we can minimize a single dipole with the local field very quickly. Calculating the strain at a point takes a time of order N, the number of dipoles, and we can then analytically diagonalize the 3×3 matrix to find the eigenvector corresponding to the largest eigenvalue. In contrast, if we were to minimize the energy along some arbitrary line in phase space, calculating the energy at a given point takes time of order N^2. This must be calculated repeatedly, since we then have to minimize the function numerically along this line. Even though this method takes a much smaller number of minimizations, each minimization is so much more time consuming that it ends up taking more time.

[23]The sum in Eq. (14) is conditionally convergent; to make it converge we use a smooth cutoff function $C(s)$, where $C(0)=1$ and $C(s)\to0$ as $s\to\infty$. Then,

$$J_{ijkl}(\mathbf{x})=\bar{\epsilon}_{ijkl}(0)+\lim_{\alpha\to0}\sum_{\mathbf{k}} C(\alpha k)\bar{\epsilon}_{ijkl}(\mathbf{k})e^{i\mathbf{k}\cdot\mathbf{x}},$$

where $\alpha=k_M^{-1}$ is the reciprocal of the largest k value used. Larger values of k_M are used until the J_{ijkl} converge. In practice, it is not too difficult to get the sum to converge using only moderately large values of k_M.

[24]In general, for thermodynamic stability, it is necessary that $\mu>0$ and $\lambda+\frac{2}{3}\mu>0$.

[25]See, e.g., I. F. Silvera, Rev. Mod. Phys. **52**, 393 (1980).

[26]M. Meissner, W. Knaak, J. P. Sethna, K. S. Chow, J. J. DeYoreo, and R. O. Pohl, Phys. Rev. B **32**, 6091 (1985).

[27]J. P. Sethna and K. S. Chow, Phase Trans. **5**, 317 (1985); J. P.

Sethna, Ann. N.Y. Acad. Sci. **484**, 130 (1986).

[28]F. Lüty and J. Ortiz-Lopez, Phys. Rev. Lett. **50**, 1289 (1983).

[29]C. I. Nicholls, L. N. Yadon, D. G. Haase, and M. S. Conradi, Phys. Rev. Lett. **59**, 1317 (1987).

[30]From $Q_0=2\mu V_0\lambda_s$ (see II, Sec. VII) we estimate $Q_0\simeq 1.3$ eV, using the shape factor $\lambda_s\simeq 0.2$, measured by H. U. Beyeler, Phys. Rev. B **11**, 3078 (1975), the volume of the primitive cell, $V_0=72$ Å^3, and approximating $\mu\simeq 7.3\times 10^{10}$ dyn/cm^2 for KBr. This value of μ is obtained by the Reuss average (see Ref. 17, p. 299), which is the spherical average of the compliance tensor of KBr (which has cubic symmetry). The Voigt average, which is an average of the elastic moduli, yields an estimate of $\mu\simeq 10.4\times 10^{10}$ dyn/cm^2, with a correspondingly higher estimate of Q_0.

[31]We will show in II that the low-frequency measured elastic constants are softened from the "bare," high-frequency values (used in the simulation) due to the phonon-defect coupling. To calculate this softening it is necessary to know the parameter $\Upsilon=Q_0^2/I$, where I is the moment of inertia. For the dielectric-loss plots shown here, we have used $\Upsilon=1.1\times 10^{15}$ ergs/sec^2, so that $I=4.0\times 10^{-39}$ gm cm^2 for $Q_0=1.3$ eV. This moment of inertia for a cyanide in a KBr host is consistent with experiment. From Beyeler's measurement (see Ref. 30) of the rotational constant, we find $I=2.8\times 10^{-39}$ gm cm^2, though R. Spitzer (Ph.D. thesis, Cornell University, Ithaca, NY, 1987) estimates $I=6.5\times 10^{-39}$ gm cm^2.

[32]K. H. Michel and J. M. Rowe, Phys. Rev. B **22**, 1417 (1980).

[33]D. Sahu and S. D. Mahanti, Phys. Rev. B **26**, 2981 (1982).

[34]K. H. Michel, Phys. Rev. B **35**, 1405 (1987); **35**, 1414 (1987).

[35]L. J. Lewis and M. L. Klein, Phys. Rev. Lett. **57**, 2698 (1986); **59**, 1837 (1987).

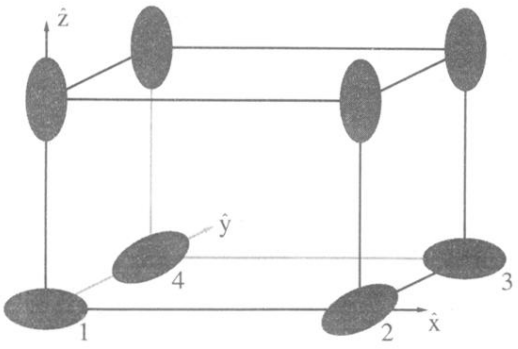

FIG. 1. Elastic dipoles are frustrated in a three-dimensional Bravais lattice.